

Learning non-rigid surface reconstruction from spatio-temporal image patches

Matteo Pedone, Abdelrahman Mostafa and Janne Heikkilä

Center for Machine Vision Research and Signal Analysis, University of Oulu, Finland

{matteo.pedone, abdelrahman.mostafa, janne.heikkila}@oulu.fi

Abstract—We present a method to reconstruct a dense spatio-temporal depth map of a non-rigidly deformable object directly from a video sequence. The estimation of depth is performed locally on spatio-temporal patches of the video, and then the full depth video of the entire shape is recovered by combining them together. Since the geometric complexity of a local spatio-temporal patch of a deforming non-rigid object is often simple enough to be faithfully represented with a parametric model, we artificially generate a database of small deforming rectangular meshes rendered with different material properties and light conditions, along with their corresponding depth videos, and use such data to train a convolutional neural network. We tested our method on both synthetic and Kinect data and experimentally observed that the reconstruction error is significantly lower than the one obtained using other approaches like conventional non-rigid structure from motion.

I. INTRODUCTION

The human visual system has a remarkable ability of discerning the three-dimensional shape of an observed scene. Although its internal mechanisms are still not entirely clear, it is known that our visual system relies simultaneously on several cues to perceive shape [27], such as the local changes in shading and texture of an object, or the temporal change in appearance of an object while seen from different angles. Researchers in the last few decades have attempted with varying degrees of success to formulate mathematical models that would approximately describe such mechanisms in order to emulate them on machines. Some of the most prominent outcomes of these efforts are: algorithms for *structure from motion* (SfM) [32], *photometric stereo* (PS) [34], *shape from shading* [16], and *shape from texture* [5], where the last two mainly focus on the special case of inferring shape from a single image. Each of these methods has a vast literature of its own. Interesting

surveys can be found in [23], [1], [25]. All the aforementioned methods have been typically approached under the strong assumption that the observed scene is static. In recent years, we have witnessed an increasing interest in extending such techniques to the case of dynamic scenes made of rigidly and non-rigidly moving objects. However, there are currently still many challenges to be faced due to the ill-posedness of the inverse problems related to the estimation of three-dimensional shape of a dynamic scene from two-dimensional images. In photometric stereo, one or more images of the same subject need to be acquired under different illuminations in order to estimate its 3D shape, and some authors have addressed the problem of moving objects by using specialized hardware [12], [17], [33]. In addition to that, the physical surface of the observed object is assumed to have certain reflectance properties (usually Lambertian). Similarly, in SfM it is assumed that the spatial coordinates in the image plane of some interest points are acquired from several point of views, and under the assumption of a static scene, the geometric relationships between corresponding points can be utilized to recover the original 3D structure of the scene. The more general problem of non-rigid structure from motion (NRSfM) considers the case where the scene itself can move non-rigidly, hence such geometric relationships become more difficult to exploit. Researchers have introduced priors on the camera model [7], on the type of trajectories of points in space-time [3], or on the shape of the object [7], [18], [11], [31], [35], [19] in order to make the problem mathematically tractable. Algorithms for NRSfM mainly differ from each other in terms of the prior they impose on the shape and motion of the objects, however currently, most methods rely on the assumption that the scene is observed through an orthographic camera (see Chapter 5 of [26] for some exceptions using the perspective camera model), and they are essentially generalizations of the popular *factorization method*, which was originally employed for traditional orthographic SfM [30]. The same assumption of orthographic camera model is made in most photometric stereo algorithms as well. From a mathematical point of view, dynamic PS and NRSfM aim at solving different problems: the former relies on pixel intensities from the images under different illuminations and returns normal maps representing surfaces in 3D space, while the latter takes a set of trajectories of tracked points in the image plane, and estimates their corresponding representation in 3D space, as well as the trajectory of the camera. Despite this fact, there exist some aspects of overlap between these two methods which motivate

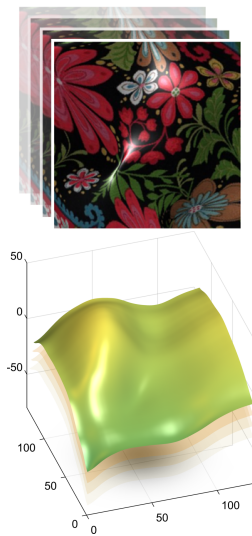


Fig. 1. Frames of a $256 \times 256 \times 16$ video of a non-rigidly deforming object and the corresponding depth maps obtained directly from the video after training a CNN with a synthetically generated database.

our work.

Although both dynamic PS and NRSfM differ significantly in terms of the inputs they rely on and of the outputs they produce, we can nonetheless argue that NRSfM algorithms are often preceded by tracking algorithms that in fact rely on information extracted from the pixel values of a video sequence. Given the recent success of deep-learning algorithms in many different settings, it is natural to investigate the feasibility of a deep-learning based approach that operates directly on a video sequence as its input, and that would automatically yield a dense representation of the scene depth for each frame. This has potentially the advantage of overcoming the frequently imposed assumptions on the illumination conditions of the scene and on the reflectance properties of the observed object (as in PS), and that of avoiding to explicitly solve the factorization problem, as in NRSfM.

The main challenge is clearly represented by the difficulty of acquiring large scale training data in which each sample would consist of a video sequence of an object (or a portion of it), along with its corresponding 3D representation in space. Although nowadays it is theoretically possible to acquire RGB video sequences along with their corresponding depth maps using inexpensive equipment, producing a sufficiently large database involving non-rigid motion of many different subjects, materials, textures, and light conditions would be a daunting and time consuming process.

In this manuscript, we try to address this problem by showing that it is possible to generate an artificial database consisting of short rendered video sequences, each depicting the movement of a small patch of a non-rigidly deforming object, along with the corresponding depth video, and then train a convolutional neural network to perform the direct estimation of a depth video from the pixel intensities of a video sequence.

The contributions of this paper are the following ones: first, we propose a simple and computationally fast mathematical model to generate the local spatio-temporal geometry of non-rigidly deforming surfaces, which can be used to form a database of rendered video clips along with their corresponding depths. Secondly, we propose a network architecture to estimate the depth map for each frame of a video sequence of a deforming object; thirdly, since the rendered scenes with an orthographic camera model are often ambiguous with respect to stretches, shears and translations along the optical axis, we derive a complete invariant for this family of transformations that is used to formulate a loss function in the training stage that implicitly operates on equivalence classes of depth maps under such transformations.

The rest of this manuscript is organized as follows. Section III describes the proposed method from a general point of view and introduces the main assumptions that are invoked in the next sections. In Section IV we provide the details related to the generation of our artificial database of spatio-temporal patches with their corresponding ground-truth depth video. Sections V-VII contain the mathematical details related to the estimation of the depth video, while the architecture of the convolutional neural network (CNN) utilized for 3D shape estimation is described in Section VI. Sections VIII and IX

respectively show the experimental results and give concluding remarks.

II. RELATED WORK

There are some recent works in the literature that can be considered related to ours. Kumar et al. [21] recently proposed a method based on superpixels and motion constraints in order to produce animated depth maps for a video sequence of moving subjects. Their method does not rely on machine learning and the estimated depth maps are always piecewise planar within the superpixel boundaries, affecting the accuracy of the reconstruction. In [8] a deep-learning based approach is presented to estimate the 3D scene flow from a 2D video. However the main application domain is road traffic navigation, and the scene is assumed to be approximately decomposable into flat planes, while the motion of the objects is assumed to be rigid. Agudo et al. shows in [2] that it is feasible to solve the NRSfM problem from video frames of an orthographic monocular camera if one assumes that the non-rigid motion can be accurately described by the equations governing the motion of elastic bodies. After determining the 3D locations of the tracked points, the authors propose a scheme to construct a triangular mesh approximating the global shape of the surface. Despite the promising results of existing methods, to the best of our knowledge, there are still no approaches entirely based on deep-learning that attempt to reconstruct the deforming surface of a non-rigidly moving object directly from a sequence of images.

III. OVERVIEW OF THE PROPOSED METHOD

We consider the problem of reconstructing the spatio-temporal depth map (depth video) from the video sequence of a non-rigidly moving object seen from a static orthographic camera. Our approach relies on the following assumptions:

- 1) The scene/object is observed by a static orthographic camera.
- 2) The deformation of the object observable within fixed spatio-temporal windows of the video sequence is non-negligible.
- 3) Locally, the 4D structure of the object (i.e. its 3D shape evolving in time) can be approximated with a parametric model controlled by a relatively small amount of parameters.

Note that these assumptions, despite being restrictive, are analogous to the assumptions made by current state-of-the-art NRSfM methods [20], [21]. The proposed method essentially consists in estimating the depth video locally, within local “patches” in the space-time domain, and then in reconstructing the entire depth map of the scene by “stitching” together the local depth videos. The estimation is done by training a neural network to learn the animated depth map within small spatio-temporal patches of a video that have size 64×64 pixels \times 16 frames in our implementation. Given the practical difficulty of acquiring a large amount of real data consisting of small video clips of deforming subjects, along with their corresponding depth videos, we generate a database of synthetic data, i.e. deforming planar meshes rendered with variable textures,

reflectance properties, and light conditions, and we obtain their respective depth videos through ray casting [24]. The database is utilized to train a CNN to directly estimate $64 \times 64 \times 16$ depth videos from RGB video sequences of the same size. In the final step, the depth videos of each patch are combined together in order to reconstruct the entire depth video. The reconstruction scheme that we utilize is inspired by the well-known method of signal reconstruction using the constant overlap-add (COLA) decomposition. Note that the assumption of orthographic camera removes the need to train the network with different camera parameters, however it introduces also an ambiguity problem where same video sequences may correspond to different depth maps. This issue is addressed in detail in Section V.

IV. ARTIFICIAL DATASET GENERATION

Consider a smooth spatio-temporal image patch $f : (-1, 1)^2 \times (0, 1) \rightarrow \mathbb{R}^3$ having the following form:

$$f(\mathbf{x}, t) = E_t(\mathbf{x} + d(\mathbf{x}, t)) \quad (1)$$

The quantity inside brackets in (1) can be interpreted as a 2D surface in \mathbb{R}^3 obtained by applying a displacement to each point of the domain of f . This essentially models a

surface obtained by applying a vector displacement (i.e. a displacement in each of the three directions) to each point of the bi-unit square. E_t are Euclidean transformations (rotations) smoothly parametrized by t that change the orientation and position of the patch. Let us denote $\mathcal{G}_\Sigma(\mathbf{u}) = e^{-\mathbf{u}^T \Sigma \mathbf{u}}$ as the two-dimensional Gaussian function where Σ is a 2×2 symmetric positive definite matrix, and a vector-valued function $\varphi(\mathbf{u}, t)$ as:

$$\varphi(\mathbf{u}, t) = \begin{bmatrix} \cos(t\phi_1(\mathbf{u}) + \theta_1(\mathbf{u})) \\ \cos(t\phi_2(\mathbf{u}) + \theta_2(\mathbf{u})) \\ \cos(t\phi_3(\mathbf{u}) + \theta_3(\mathbf{u})) \end{bmatrix} \quad (2)$$

$$d(\mathbf{x}, t) = \kappa \mathcal{G}_\nu(\mathbf{x}) \text{diag}(\zeta, \zeta, 1) \mathcal{F}^{-1} \{w \mathcal{G}_\xi \mathcal{G}_\Sigma \varphi(\cdot, t)\}(\mathbf{x}) \quad (3)$$

where \mathcal{F}^{-1} is the inverse 2D Fourier transform operator applied “channel-wise”, and $w : (\mathbb{R}_{\geq 0})^2 \rightarrow [0, 1]$ is a 2-dimensional circular symmetric function whose radial profile is rapidly increasing, and such that $w(\mathbf{0}) = 0$, which guarantees that the integral of d is zero. The scalar parameters κ (*intensity*), ν (*constraint*), ζ (*folding*), ξ (*flexibility*), respectively control the overall strength of the displacement, how much the square patch remains anchored at its border, how much it tends to create folds, and how much it behaves like a soft or hard surface. The matrix Σ controls the distribution of *orientations* of the displacements, while $\phi, \theta : \mathbb{R}^2 \rightarrow \mathbb{R}^3$ are functions that determine the speed by which each frequency component changes in time and their initial phase angle (Figure 3). Our approach of defining a moving surface by

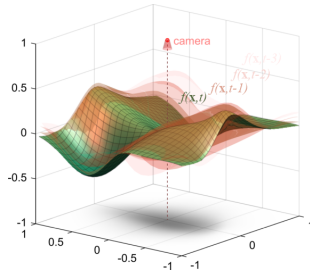


Fig. 2. Graphical illustration of a spatio-temporal patch f in (1)

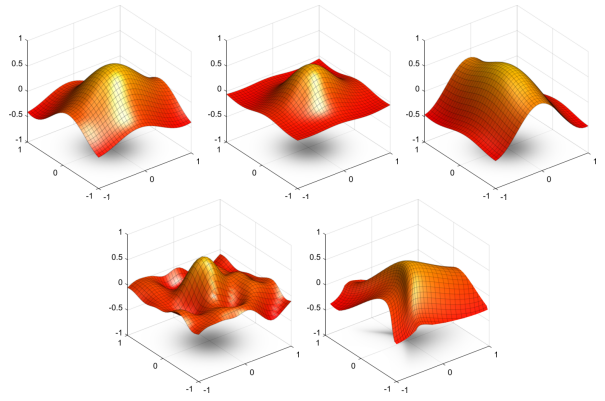


Fig. 3. Illustration of the effect of the parameters of (3). From left to right, top to bottom: a patch obtained by setting ν, ζ, ξ to very low values and $\Sigma = I$. The same patch with increased *constraint*. With non-identity Σ . With increased *flexibility*. With increased *folding*.

means of (3) can be seen as a computationally cheap way to emulate the appearance of a planar surface with given physical properties, animated by means of realistic cloth simulation. We argue that in our application it is not strictly necessary to obtain physical correctness of the movement, thus we adopt the strategy of using colored noise to generate the geometry of the patch and its movement. Analogous strategies are often encountered in the literature of computer graphics, especially in application related to realistic real-time rendering of fluids, e.g. [29]. Note that in a practical scenario, the domain of f would be obviously discretized into a 3D array. After the geometry of a moving patch is defined, we render 153600 video clips of moving patches f by varying the parameters in (3), the light source parameters, the texture of the surface, its reflectance properties, and the variance of the noise that is added after the render. For rendering, we adopt the Phong reflectance model. More accurate reflectance models could be used to increase realism, at the expenses of computational speed and parameters to handle. The textures that we use in our implementation are 256×256 crops extracted at random position from the images of the DTD database [10]. The render pass produces for each clip a stack of $16 \times 64 \times 64$ pixels that we call f_{render} . In addition to the render pass, we use ray casting [24] to produce another $64 \times 64 \times 16$ array f_{depth} of corresponding depth maps (Figure 4). A single database entry is represented by a pair (f_{render}, f_{depth}) .

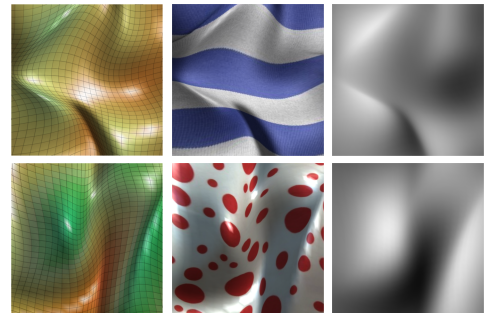


Fig. 4. Two examples of scenes rendered with our method. From left to right, the 3D mesh, rendered object, and depth map are depicted.

V. AMBIGUITY-INVARIANT REPRESENTATION OF DEPTH MAPS

Adopting an orthographic camera model has the advantage of avoiding the need to train the network with different camera parameters, however scenes rendered with orthographic projection are prone to ambiguities. In the particular case of Lambertian surfaces illuminated by directional light sources, the resulting ambiguity is the *generalized bas-relief ambiguity* (GBR) [6], that has been studied extensively in the context of *shape from shading*, and which is essentially a composition of shears and stretches along z , the optical axis. Although the rendered surfaces in our database are not always perfectly Lambertian, the reflectance model adopted in the rendering stage is not sufficient to resolve entirely the ambiguity, even in presence of texture and specular highlights. Therefore, any rendered scene in our database is virtually indistinguishable from all the other hypothetical rendered scenes undergoing an arbitrary GBR transformation. This issue would surely impair the training stage, hence it is crucial to find a representation of smooth depth map surface that is invariant to the GBR transformation. Once, such an invariant representation is obtained, it is possible to utilize it in the loss function of the training stage of the network. This has the big advantage of letting the network treat all the GBR-transformed versions of one depth map as an entire equivalence class: in fact, the invariants of two depth maps related by a GBR transformation will be exactly the same, hence the loss function will yield always zero in such cases.

Let us consider the space \mathcal{S} of smooth surfaces (spatial patches) $f: \mathbb{R}^2 \rightarrow \mathbb{R}^3$ defined as follows, and denote with \tilde{f} a GBR-transformed version of f :

$$f(x, y) = \begin{bmatrix} x \\ y \\ z(x, y) \end{bmatrix} \quad (4)$$

$$\tilde{f} = \begin{bmatrix} \tilde{x} \\ \tilde{y} \\ \tilde{z} \end{bmatrix} = \begin{bmatrix} x \\ y \\ \alpha x + \beta y + \lambda z + \tau \end{bmatrix}$$

where $z \in C^\infty(\mathbb{R}^2)$ is the corresponding depth map, $\alpha, \beta, \tau \in \mathbb{R}$, and $\lambda \in \mathbb{R}^+$. In order to find a representation for an arbitrary f that is invariant to the group of GBR transformations, we use the *normalization construction* [22], which is a well-known technique in classical invariant theory that enables us to algorithmically derive complete differential invariants for the action of the GBR transformations on depth maps. We thus make the following statement (its proof can be found in the supplementary material):

Theorem 1. *Given a surface $f \in \mathcal{S}$, the quantity*

$$\iota_f := \frac{\nabla^2 z}{\|\nabla^2 z\|_F} \quad (5)$$

where ∇^2 and $\|\cdot\|_F$ denote respectively the Hessian and the Frobenius norm, is a complete differential invariant for f with respect to the action of the GBR transformations.

In our application we consider also another complete invariant for the subgroup of the GBR transformations given

by scaling and translations along z , and obtained from (4) by setting $\alpha = \beta = 0$.

Theorem 2. *Given a surface $f \in \mathcal{S}$, the quantity*

$$\eta_f := \|\nabla^2 z\|_F^{-1} (\nabla z, \nabla^2 z) \quad (6)$$

where ∇, ∇^2 are respectively the gradient and Hessian operators, is a complete differential invariant for f with respect to stretches and translations along z .

Note that in a practical implementation, the partial derivatives of z in (5)-(6) would need to be estimated with first and second derivative filters.

VI. NETWORK ARCHITECTURE

In order to estimate a depth video from its corresponding sequence of grayscale video frames, we use an architecture similar to the 3D U-net [9] (see Figure 5). The input for the network is a 16 frames video and each frame size is 64×64 pixels. The output of the network is the corresponding depth video, which has size $32 \times 32 \times 16$. To enlarge the receptive field and get richer features, a context module [36] with Atrous spatial pyramid pooling is introduced which performs parallel dilated convolutions with different dilation rates. These feature maps are then concatenated, and the output of the module is the convolution of these feature maps. For the first two stages in the network, three dilation rates are used (1, 2, 3). For the following two stages, two dilation rates are used (1, 2) as the feature maps dimensions get smaller. We use $3 \times 3 \times 3$ kernels for all convolutions. The *leaky ReLU* activation function is used for all layers, except for the last one, which has a *linear* activation function to predict the depths.

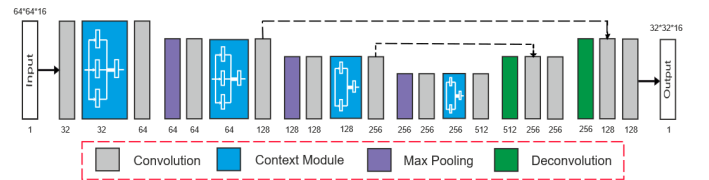


Fig. 5. The network architecture: the input is a grayscale video and the output is the corresponding sequence of depth maps. Below each layer the number of channels is reported.

VII. RECONSTRUCTION OF A DEPTH MAP FROM LOCAL PATCHES

The proposed network architecture is designed to recover only depth videos whose frames have dimension 64×64 . When the input video has larger dimensions, an additional step is required in order to reconstruct the full-sized depth map from the local patches. To address this issue we split a frame of the input video into 64×64 squares with constant overlap and run our algorithm to estimate the depth in each block. Since the recovered depth maps are ambiguous with respect to a GBR transformation, we also run our algorithm on a version of the input video downsized along the spatial dimension to 64×64 . This yields depth maps that represent a coarse representation of the full-sized depth map. We upscale the

	ℓ_{tr+sc}	ℓ_{GBR}
align each frame	0.4258 ± 0.1384	0.3832 ± 0.1305
alignment from 1st frame	0.6657 ± 0.2718	0.6133 ± 0.259

TABLE I

AVERAGE AND STANDARD DEVIATION OF MAE-SN CALCULATED FROM 15360 VIDEO SEQUENCES FOR THE TWO LOSS FUNCTIONS CONSIDERED.

coarse depth map to the original size of the video frames, and to each 64×64 patch we apply the best (in least square sense) GBR transformation that aligns it with the corresponding patch in the coarse level. The resulting patches are then multiplied by a two-dimensional triangle function (i.e. the outer product of a triangle function with itself) and added together. Note that such a reconstruction scheme has strong analogies with the well-known constant overlap-add (COLA) reconstruction often seen in the context of reconstruction of signals from their short-time Fourier transform [4]. The temporal dimension is processed in an analogous way.

VIII. EXPERIMENTS

In order to validate our method we performed three experiments. In the first one, we generated a database of 153600 entries as explained in Section IV. We split it into three partitions: 80% for training, 10% for validation, 10% for testing, and use it to train a CNN with the architecture described in Section VI. For training, we tried two loss functions: $\ell_{GBR} = \text{MSE}(\iota_f, \iota_{f^*})$ and $\ell_{tr+sc} = \text{MSE}(\eta_f, \eta_{f^*})$, where f, f^* are respectively the estimated and ground truth depth maps. Since both invariants can be degenerate at some locations, we consider only those pixels where the quantities are defined. To quantitatively evaluate the performance we align the estimated depth maps with the corresponding ground truth by a linear transformation and calculate the *mean absolute spatially-normalized error* $\text{MAE-SN} = T^{-1} \sum_{t=1}^T \sigma_{f^*(\cdot, t)}^{-1} \text{MAE}(f(\cdot, t), f^*(\cdot, t))$, which is scale-invariant in the spatial dimensions. We also repeat the same experiment by re-using the parameters for the alignment of the first frame for all the other frames. The results are summarized in Table I.

In the second experiment we synthetically generate 1000 samples (f_{render}, f_{depth}) having size $256 \times 256 \times 16$ using the method in Section IV and use significantly different parameters in Equation (3) than the ones used in the training stage. We then automatically select 1089 points scattered uniformly on the 3D mesh and track their xy -coordinates on the image plane. We use these coordinates as inputs for two popular state-of-the-art NRSfM methods: CSF2 [15], and KSTA [14], and obtain the z -coordinates of the tracked points for each frame. To obtain a dense 256×256 depth map we use scattered interpolation at each frame and then apply a linear transformation to the estimated depth maps to align them with the respective ground-truths and calculate the MAE-SN of each depth video. We finally compare the results with the depth videos obtained directly from the video sequences using our method. Since the videos have larger dimensions than the ones used in training, we apply the strategy described in Section VII to obtain full-sized depth videos. The results are summarized in Table II.

ours with ℓ_{GBR}	CSF2 [15]	KSTA [14]
0.5907 ± 0.4536	0.8746 ± 0.6372	0.8738 ± 0.6369

TABLE II

AVERAGE AND STANDARD DEVIATION OF MAE-SN CALCULATED FROM 1000 VIDEO SEQUENCES USING OUR METHOD AND TWO STATE-OF-THE-ART NRSfM RECONSTRUCTION ALGORITHMS.

ours with ℓ_{GBR}	CSF2 [13]	KSTA [14]
3.7	4.6	4.3

TABLE III

AVERAGE AND STANDARD DEVIATION OF MAE (IN MILLIMETERS) CALCULATED FROM A REAL VIDEO SEQUENCE USING OUR METHOD AND TWO STATE-OF-THE-ART NRSfM RECONSTRUCTION ALGORITHMS.

In the third experiment we used real data, where 25 frames of grayscale video and the corresponding depth maps were acquired using Microsoft Kinect 1 pointed to the shirt of a moving person in an indoor environment. A fixed region of interest (64×64 pixels) was manually chosen, where details were visible and depth pixels were defined, thus the whole input video sequence has size $64 \times 64 \times 25$. For our method, we estimate the depth videos directly from the video sequence, as done in the previous experiments (Figure 6). To obtain the input for CSF2 and KSTA algorithms, we performed point tracking on the two video sequences using the minimum eigenvalue algorithm [28], which yielded the highest amount of correctly tracked points (31) and manually calibrated their parameters to obtain best results. The depth videos were obtained as in the previous experiment. The results are given in Table III.

IX. CONCLUSION

We presented a deep-learning based approach to recover a depth video directly from a video sequence of a non-rigidly deforming object. We addressed the problem of training the network by synthetically generating a large database of short videos depicting deforming 3D meshes rendered with realistic textures, and paired with their corresponding depth videos. We tested our method on both synthetic and real videos and experimentally observed that the quality of the estimated depth videos outperforms that of state-of-the-art NRSfM algorithms.

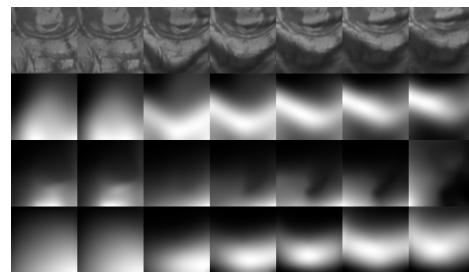


Fig. 6. *First row*: seven frames extracted from a video sequence depicting a detail of a shirt on a moving person. *Second row*: ground truth depth maps obtained with Kinect 1. *Third row*: depth maps recovered with KSTA [14] (CSF2 [15] produced visually similar results). *Last row*: depth maps recovered with our method. The contrast of the depth maps in the figure was enhanced for visualization purposes.

APPENDIX

In this Appendix we provide a proof of Theorem 1. Since $\tilde{x} = x$ and $\tilde{y} = y$, we can concentrate the discussion on \tilde{z} . Consider the n -th order *prolongation* of \tilde{z} at an arbitrary point of \mathbb{R}^2 :

$$\tilde{z}^{[n]} = [\tilde{z} \quad \tilde{z}_x \quad \tilde{z}_y \quad \tilde{z}_{xx} \quad \tilde{z}_{xy} \quad \tilde{z}_{yy} \quad \dots] \in \mathbb{R}^{[n]} \quad (7)$$

where the rightmost term is an element of a real vector space $\mathbb{R}^{[n]}$ having as many dimensions as the number of partial derivatives of z of order less than or equal to n . Consider the following system of *normalization equations*:

$$\begin{cases} \tilde{z} & = 0 \\ \tilde{z}_x & = 0 \\ \tilde{z}_y & = 0 \\ \tilde{z}_{xx}^2 + \tilde{z}_{xy}^2 + \tilde{z}_{yx}^2 + \tilde{z}_{yy}^2 & = 1 \end{cases} \quad (8)$$

By plugging the explicit formulas for the partial derivatives in (7) into (8) and solving for the parameters $\alpha, \beta, \lambda, \tau$ one obtains:

$$\begin{aligned} \alpha &= -\frac{z_x}{\|\nabla^2 z\|_F} \\ \beta &= -\frac{z_y}{\|\nabla^2 z\|_F} \\ \lambda &= \|\nabla^2 z\|_F^{-1} \\ \tau &= -[\alpha \quad \beta \quad \lambda] f \end{aligned} \quad (9)$$

The equations in (9) are called *moving frame* and plugging the parameter values of the moving frame into (7) yields a differential invariant for the action of G :

$$I_f = \frac{1}{\|\nabla^2 z\|} [0 \quad 0 \quad 0 \quad z_{xx} \quad z_{xy} \quad z_{yx} \quad z_{yy} \quad \dots] \quad (10)$$

It is possible to verify, that the entries of I_f that contain derivatives of degree higher than 2 are obtainable from the firsts three non-zero invariants in (10). Furthermore, we recognize $z_{xx}, z_{xy}, z_{yx}, z_{yy}$ as the entries of the 2×2 Hessian matrix of z , therefore we can conclude that a complete differential invariant for the action of G on \mathcal{S} is given by:

$$\iota_f = \frac{1}{\|\nabla^2 z\|_F} \begin{bmatrix} z_{xx} & z_{xy} \\ z_{yx} & z_{yy} \end{bmatrix} = \frac{\nabla^2 z}{\|\nabla^2 z\|_F}$$

ACKNOWLEDGEMENTS

The authors would like to thank Prof. Peter J. Olver for his technical advice and elucidations on the theory of the moving frame, and Academy of Finland for the financial support for this research (grant no. 297732).

REFERENCES

- [1] Jens Ackermann and Michael Goesele. A Survey of Photometric Stereo Techniques. *Foundations and Trends® in Computer Graphics and Vision*, 9(3-4):149–254, November 2015.
- [2] Antonio Agudo, Francesc Moreno-Noguer, Begoña Calvo, and J. M. M. Montiel. Sequential Non-Rigid Structure from Motion Using Physical Priors. *IEEE Transactions on Pattern Analysis and Machine Intelligence*, 38(5):979–994, May 2016.
- [3] I. Akhter, Y. Sheikh, S. Khan, and T. Kanade. Trajectory Space: A Dual Representation for Nonrigid Structure from Motion. *IEEE Transactions on Pattern Analysis and Machine Intelligence*, 33(7):1442–1456, July 2011.
- [4] J.B. Allen and L.R. Rabiner. A unified approach to short-time Fourier analysis and synthesis. *Proceedings of the IEEE*, 65(11):1558–1564, November 1977.
- [5] J. Aloimonos. Shape from texture. *Biological Cybernetics*, 58(5):345–360, April 1988.
- [6] P.N. Belhumeur, D.J. Kriegman, and A.L. Yuille. The bas-relief ambiguity. In *Proceedings of IEEE Computer Society Conference on Computer Vision and Pattern Recognition*, pages 1060–1066, San Juan, Puerto Rico, 1997. IEEE Comput. Soc.
- [7] C. Bregler, A. Hertzmann, and H. Biermann. Recovering non-rigid 3D shape from image streams. In *Proceedings IEEE Conference on Computer Vision and Pattern Recognition. CVPR 2000 (Cat. No.PR00662)*, volume 2, pages 690–696 vol.2, June 2000.
- [8] Fabian Brickwedde, Steffen Abraham, and Rudolf Mester. Mono-SF: Multi-View Geometry Meets Single-View Depth for Monocular Scene Flow Estimation of Dynamic Traffic Scenes. *arXiv:1908.06316 [cs]*, August 2019.
- [9] Özgün Çiçek, Ahmed Abdulkadir, Soeren S Lienkamp, Thomas Brox, and Olaf Ronneberger. 3D U-Net: Learning dense volumetric segmentation from sparse annotation. In *International Conference on Medical Image Computing and Computer-Assisted Intervention*, pages 424–432. Springer, 2016.
- [10] M. Cimpoi, S. Maji, I. Kokkinos, S. Mohamed, and A. Vedaldi. Describing Textures in the Wild. In *Proceedings of the IEEE Conf. on Computer Vision and Pattern Recognition (CVPR)*, 2014.
- [11] Yuchao Dai, Huizhong Deng, and Mingyi He. Dense Non-rigid Structure-from-Motion Made Easy - A Spatial-Temporal Smoothness based Solution. *arXiv:1706.08629 [cs]*, June 2017.
- [12] Graham Fyffe, Xueming Yu, and Paul Debevec. Single-shot photometric stereo by spectral multiplexing. In *2011 IEEE International Conference on Computational Photography (ICCP)*, pages 1–6, April 2011.
- [13] P. F. U. Gotardo and A. M. Martinez. Kernel non-rigid structure from motion. In *2011 International Conference on Computer Vision*, pages 802–809, November 2011.
- [14] Paulo F. U. Gotardo and Aleix M. Martinez. Kernel non-rigid structure from motion. In *2011 International Conference on Computer Vision*, pages 802–809, Barcelona, Spain, November 2011. IEEE.
- [15] Paulo F.U. Gotardo and Aleix M. Martinez. Non-rigid structure from motion with complementary rank-3 spaces. In *CVPR 2011*, pages 3065–3072, June 2011.
- [16] Katsushi Ikeuchi and Berthold K. P. Horn. Numerical shape from shading and occluding boundaries. *Artificial Intelligence*, 17(1):141–184, August 1981.
- [17] Hyeonwoo Kim, Bennett Wilburn, and Moshe Ben-Ezra. Photometric Stereo for Dynamic Surface Orientations. In Kostas Daniilidis, Petros Maragos, and Nikos Paragios, editors, *Computer Vision – ECCV 2010*, Lecture Notes in Computer Science, pages 59–72, Berlin, Heidelberg, 2010. Springer.
- [18] S. Kumar, Y. Dai, and H. Li. Multi-Body Non-Rigid Structure-from-Motion. In *2016 Fourth International Conference on 3D Vision (3DV)*, pages 148–156, October 2016.
- [19] Suryansh Kumar, Anoop Cheria, Yuchao Dai, and Hongdong Li. Scalable Dense Non-rigid Structure-from-Motion: A Grassmannian Perspective. *arXiv:1803.00233 [cs]*, March 2018.
- [20] Suryansh Kumar, Anoop Cheria, Yuchao Dai, and Hongdong Li. Scalable Dense Non-Rigid Structure-From-Motion: A Grassmannian Perspective. In *Proceedings of the IEEE Conference on Computer Vision and Pattern Recognition*, pages 254–263, 2018.
- [21] Suryansh Kumar, Ram Srivatsav Ghorakavi, Yuchao Dai, and Hongdong Li. Dense Depth Estimation of a Complex Dynamic Scene without Explicit 3D Motion Estimation. *arXiv:1902.03791 [cs]*, March 2019.
- [22] Peter J Olver. *Classical Invariant Theory*, volume 44. Cambridge University Press, 1999.
- [23] Onur Ozyesil, Vladislav Voroninski, Ronen Basri, and Amit Singer. A survey of structure from motion. *Acta Numerica*, 26:305–364, May 2017.
- [24] Scott D Roth. Ray casting for modeling solids. *Computer Graphics and Image Processing*, 18(2):109–144, February 1982.
- [25] Ruo Zhang, Ping-Sing Tsai, J.E. Cryer, and M. Shah. Shape-from-shading: A survey. *IEEE Transactions on Pattern Analysis and Machine Intelligence*, 21(8):690–706, August 1999.
- [26] Mathieu Salzmann and Pascal Fua. Deformable Surface 3D Reconstruction from Monocular Images. *Synthesis Lectures on Computer Vision*, 2(1):1–113, December 2010.
- [27] Linda G. Shapiro and George C. Stockman. *Computer Vision*. Prentice Hall, Upper Saddle River, NJ, 2001.

- [28] Jianbo Shi and Tomasi. Good features to track. In *1994 Proceedings of IEEE Conference on Computer Vision and Pattern Recognition*, pages 593–600, June 1994.
- [29] Jerry Tessendorf et al. Simulating ocean water. *Simulating nature: realistic and interactive techniques. SIGGRAPH*, 1(2):5, 2001.
- [30] Carlo Tomasi and Takeo Kanade. Shape and motion from image streams under orthography: A factorization method. *International Journal of Computer Vision*, 9(2):137–154, November 1992.
- [31] L. Torresani, A. Hertzmann, and C. Bregler. Nonrigid Structure-from-Motion: Estimating Shape and Motion with Hierarchical Priors. *IEEE Transactions on Pattern Analysis and Machine Intelligence*, 30(5):878–892, May 2008.
- [32] S. Ullman and Sydney Brenner. The interpretation of structure from motion. *Proceedings of the Royal Society of London. Series B. Biological Sciences*, 203(1153):405–426, January 1979.
- [33] George Vogiatzis and Carlos Hernández. Practical 3D Reconstruction Based on Photometric Stereo. In Roberto Cipolla, Sebastiano Battiato, Giovanni Maria Farinella, and Janusz Kacprzyk, editors, *Computer Vision*, volume 285, pages 313–345. Springer Berlin Heidelberg, Berlin, Heidelberg, 2010.
- [34] Robert J. Woodham. Photometric Stereo. Technical Report AI-M-479, MASSACHUSETTS INST OF TECH CAMBRIDGE ARTIFICIAL INTELLIGENCE LAB, June 1978.
- [35] J. Yan and M. Pollefeys. A Factorization-Based Approach for Articulated Nonrigid Shape, Motion and Kinematic Chain Recovery From Video. *IEEE Transactions on Pattern Analysis and Machine Intelligence*, 30(5):865–877, May 2008.
- [36] Shangchen Zhou, Jiawei Zhang, Wangmeng Zuo, Haozhe Xie, Jinshan Pan, and Jimmy S Ren. DAVANet: Stereo Deblurring with View Aggregation. In *Proceedings of the IEEE Conference on Computer Vision and Pattern Recognition*, pages 10996–11005, 2019.